Deformable Image Registration Using Functions of Bounded Deformation

Ziwei Nie and Xiaoping Yang

***Abstract*— Deformable image registration is a widely used technique in the field of computer vision and medical image processing. Basically, the task of deformable image registration is to find the displacement field between the moving image and the fixed image. Many variational models are proposed for deformable image registration, under the assumption that the displacement field is continuous and smooth. However, displacement fields may be discontinuous, especially for medical images with intensity inhomogeneity, pathological tissues, or heavy noises. In the mathematical theory of elastoplasticity, when the displacement fields are possibly discontinuous, a suitable framework for describing the displacement fields is the space of functions of bounded deformation (BD). Inspired by this, we propose a novel deformable registration model, called the BD model, which allows discontinuities of displacement fields in images. The BD model is formulated in a variational framework by supposing the displacement field to be a function of BD. The existence of solutions of this model is proven. Numerical experiments on 2D images show that the BD model outperforms the classical demons model, the log-domain diffeomorphic demons model, and the state-of-the-art vectorial total variation model. Numerical experiments on two public 3D databases show that the target registration error of the BD model is competitive compared with more than ten other models.**

***Index Terms*— Deformable image registration, functions of bounded deformation, variational problem, image processing.**

I. Introduction

IMAGE registration, also known as image matching, image alignment, is the process of registering two or more images of the same scene or object. This process involves designating one image as the reference (also called the reference image or the fixed image), and applying geometric transformations to the other images (called the moving images or floating images) so that they align with the reference. Registration is necessary in order to compare and analyze the data in a unified coordinate system, especially when dealing with medical images or volumes. Deformable registration has been one of the main challenges in modern medical image analysis [1]–[12]. The term deformable (as opposed to linear or global) is used to denote the fact that the observed signals are associated through a nonlinear dense transformation, or a spatially varying deformation model [1].

In general, registration can be performed on two or more images, with given colormaps like the grayscale or RGB colormap [13], [14]. For simplicity of narrative, we assume in this paper that there are only one fixed image R and one moving image M to be registered and they are both grayscale images. In addition, we assume that these two images are just in the same modality, which means that the images are obtained from the same imaging device. It is canonical to regard the intensities of these two images as functions, and without causing any confusion we still denote them as R, M, respectively. Thus R, M are defined on the image domain $\Omega \subset \mathbb{R}^d$, i.e.

$$R : \Omega \subset \mathbb{R}^d \to [0, 1], \quad M : \Omega \subset \mathbb{R}^d \to [0, 1],$$

where $d = 2, 3$ and the function range can also be $[0, 255]$ or other ranges in practice. R and M are corresponded by a transformation φ. In other words, the position $\mathbf{x}$ in R is supposed to correspond to the position $\varphi(\mathbf{x})$ in M. This transformation at every $\mathbf{x} \in \Omega$ is given as the addition of an identity transformation with the displacement field $\mathbf{u}$, i.e.

$$\varphi(\mathbf{x}) = \mathbf{x} + \mathbf{u}(\mathbf{x}),$$

where the displacement field is

$$\mathbf{u} : \Omega \to \mathbb{R}^d, \quad \mathbf{u} = (u_1, \cdots, u_d)^T.$$

That is, we assume there exists a displacement field $\mathbf{u}$ such that the pixel $\mathbf{x} \in \Omega$ of the fixed image R and the pixel $\mathbf{x}+\mathbf{u}(\mathbf{x}) \in \Omega$ of the moving image M represent the same position of the concerned scene or object. Thus we can write the registration model as an optimization problem:

$$\min_{\varphi} SSD(M, R, \varphi) = \|M \circ \varphi(\mathbf{x}) - R(\mathbf{x})\|^2,$$

or

$$\min_{\mathbf{u}} SSD(\mathbf{u}) = \|M(\mathbf{x} + \mathbf{u}(\mathbf{x})) - R(\mathbf{x})\|^2.$$

It is ill-posed, mainly because the convexity of the object function remains unknown. Actually $SSD(\mathbf{u})$ is often highly non-convex due to the existence of distortions in images [2], [3].

Variational deformable registration models have been widely used and proven to be efficient and valuable [1], [2]. A general variational framework of deformable registration

Manuscript received September 28, 2018; revised December 27, 2018, January 7, 2019, January 15, 2019 and January 22, 2019; accepted January 23, 2019. Date of publication January 31, 2019; date of current version May 31, 2019. This work was supported by the National Natural Science Foundation of China under Grant 11531005 and Grant 91630311. *(Corresponding author: Xiaoping Yang.)*

Z. Nie is with the School of Science, Nanjing University of Science and Technology, Nanjing 210094, China (e-mail: 612112375@njust.edu.cn).

X. Yang is with the Department of Mathematics, Nanjing University, Nanjing 210093, China (e-mail: xpyang@nju.edu.cn).

This paper has supplementary downloadable material available at http://ieeexplore.ieee.org, provided by the author.

Color versions of one or more of the figures in this paper are available online at http://ieeexplore.ieee.org.

Digital Object Identifier 10.1109/TMI.2019.2896170

involves finding a global (more often a local) minimizer of an energy functional which consists of a data term, also known as the dissimilarity metric, and a regularization term, on the transformation or on the displacement field directly. It can be written as

$$\min_{\mathbf{u}\in\mathcal{K}} E(\mathbf{u}) = Data(M, R, \mathbf{u}) + \lambda Regu(\mathbf{u}), \tag{1}$$

where $\lambda > 0$ is a weight parameter balancing the data term and the regularization term, and $\mathcal{K}$ is an admissible set of solutions. Commonly used data terms [2], [3], [12] include the sum of squared differences (*SSD*), normalized cross correlation (*NCC*), normalized mutual information (*NMI*), local correlation coefficients (*LCC*). In this paper, we use *SSD* as the data term since it is a proper choice for registering images of the same modality and easy to compute [1], [2]. As to the regularization term, which is the focus of this paper, so far there are quite a number of choices for this variational framework, such as the L^2 norm of the displacement field [5]–[7], the L^2 norm of the gradient of the transformation [8]–[10], the vectorial total variation of the displacement field [11], [12]. Before the proposal of our model, let us briefly review these classical or state-of-the-art models.

In 1981 [4], Broit proposed to model an image grid as an elastic membrane that is deformed under the influence of two forces that compete until equilibrium is reached. An external force tries to deform the image such that matching is achieved while an internal one enforces the elastic properties of the material. According to the theory of elasticity, the Navier-Cauchy Equation is employed to describe the displacement field [1]:

$$\mu\nabla^2\mathbf{u} + (\mu + \lambda)\nabla(\nabla \cdot \mathbf{u}) + \mathbf{F} = 0, \tag{2}$$

where $\mathbf{F}(\mathbf{x})$ is the force field that drives the registration based on the registration dissimilarity measure, such as the *SSD* term. The parameter μ and λ are *Lame* constants. Actually, the above equation comes from the Euler-Lagrange equation of the following functional energy [2]:

$$E(\mathbf{u}) = Data(M, R, \mathbf{u}) + \frac{1}{2}\left(\mu\|\nabla\mathbf{u}\|^2 + (\mu+\lambda)\|\nabla\cdot\mathbf{u}\|^2\right). \tag{3}$$

Note that the elastic model obtains smooth displacement fields, which is consistent with the theory of elasticity [15].

In 1998 [5], Thirion proposed the so-called Demons model for image registration task by employing the optical flow equation of the fixed image and the moving image. Therein the registration task is treated as a diffusion process, which is typically a physical problem. Basically, we can consider Demons model in the variational framework where the regularization term is set to be $\|\mathbf{u}\|^2_{L^2}$ [6], and the data term is derived from the optical flow equation :

$$\mathbf{u}\cdot\nabla M = R - M.$$

Thus the functional energy is

$$E(\mathbf{u}) = \|M - R + \mathbf{u}\nabla M\|^2 + \lambda\|\mathbf{u}\|^2, \tag{4}$$

where $\lambda > 0$ is a given parameter. The displacement field $\mathbf{u}$ is obtained by adding up the update of each processing iteration [5], [6], followed by a Gaussian smoothing step. Thus the obtained displacement field is a vectorial smooth L^2 function, i.e. $\mathbf{u} \in W^{1,2}(\Omega, \mathbb{R}^d)$. Note that Demons model may not suit for the case of large displacement, since optical flow is used to find small displacements in temporal sequence of images [5].

In 2004 [7], Haker *et al.* considered image registration as an optimal mass transport problem. Regardless of the optimal transport theory, the registration model proposed in [7] is actually obtained by adding up an *SSD* term and a L^2-norm term of the displacement field $\mathbf{u}$. Thus the functional energy can actually be written as:

$$E(\mathbf{u}) = SSD(\mathbf{u}) + \lambda\|\mathbf{u}\|^2 = \|M(\mathbf{u}) - R\|^2 + \lambda\|\mathbf{u}\|^2, \tag{5}$$

with $\lambda > 0$. Note that this model is different from Demons model, while they are just the same if we take the first-order Taylor approximation of M, see (16).

In 2008 [8], Vercauteren *et al.* proposed a demons-based diffeomorphic registration model which solves the transformation in the log-domain (DiffeoDemons model). The main idea of the model is to represent the current transformation φ as an exponential of a smooth velocity field $\mathbf{V}$, i.e. $\varphi = exp(\mathbf{V})$, and use the diffeomorphic demons to efficiently compute an update $\mathbf{v}$ of the form $\varphi \circ exp(\mathbf{v}) = exp(\mathbf{V}) \circ exp(\mathbf{v})$. The notation exp denotes the exponential mapping in the Lie algebra (the vector space of velocity fields). Therein the functional energy is given by:

$$\begin{aligned} E(\varphi) &= SSD(M, R, \varphi) + \lambda\|\nabla\varphi\|^2 \\ &= \|M\circ\varphi - R\|^2 + \lambda\|\nabla\varphi\|^2, \end{aligned} \tag{6}$$

where $\lambda > 0$. Note that $\nabla\varphi$ above is actually the Jacobian of the transformation φ, and DiffeoDemons model ensures the displacement field to be continuous and smooth. This implies that $\mathbf{u} \in W^{1,2}(\Omega, \mathbb{R}^d)$.

In 2013 [11], Chumchob proposed a vectorial total variation-based deformable registration model (VTV model) with the data term being *SSD* and the regularization term being a vectorial total variation of the displacement field as following:

$$\|\nabla(\mathbf{u})\|_1 = \int_\Omega |\nabla\mathbf{u}| d\mathbf{x} = \int_\Omega \sqrt{\sum_{i=1}^{d} |\nabla u_i|^2} d\mathbf{x}. \tag{7}$$

Chumchob pointed out that the above regularization term is the same as that in the color image denoising models. In other words, the displacement field is considered as a vector-valued function with bounded vectorial variation, which in turn implies that all the components are ideally piecewise constant functions and $\mathbf{u} \in BV(\Omega, \mathbb{R}^d)$ [16]. We refer [17] for the detailed introduction and discussion of vectorial total variation. Note that the above regularization term is an isotropic version, since the gradients of all the components of the deformation field are mixed together and treated equally.

In 2017 [12], Vishnevskiy *et al.* used the discrete version of isotropic vectorial total variation as the regularization term for deformable image registration. *SSD* and *LCC* were employed as the data term. Therein the functional energy is given by:

$$\begin{aligned} E(\mathbf{u}) &= SSD(\mathbf{u}) + \lambda Regu(\mathbf{u}) \\ &= \|M(\mathbf{u}) - R\|^2 + \lambda\|\nabla\mathbf{u}\|_1, \end{aligned} \tag{8}$$

and

$$E(\mathbf{u}) = LCC(\mathbf{u}) + \lambda\|\nabla\mathbf{u}\|_1, \tag{9}$$

where $\lambda > 0$. Both models with *SSD* and *LCC* data terms were tested on several public 3D databases and achieved state-of-the-art performance, and the registration results showed that VTV-regularization did not oversmooth the displacement fields [12].

Except for VTV model, all the other models reviewed above obtain smooth displacement fields, which is not always the case in real-world images, especially for medical images with intensity inhomogeneity, pathological tissues or heavy noises. See the fixed and the moving images in Fig. 4, Fig. 7, and the computed displacement fields in Fig. 6, Fig. 8 for example. In the mathematical theory of elastoplasticity [15], [21], when the displacement fields are possibly discontinuous, a suitable framework for describing the displacement fields is the space of functions of bounded deformation. Inspired by this, we propose a novel deformable registration model, called BD model, which allows possible discontinuities of displacement fields in images. BD model is formulated in a variational framework by supposing the displacement field to be a function of bounded deformation. This is consistent with the theory of elastoplasticity [15], in which the following strain-displacement relations hold:

$$\varepsilon_{ij} = \frac{1}{2}\left(u_{i,j} + u_{j,i}\right) = \frac{1}{2}\left(\partial_{x_j}u_i + \partial_{x_i}u_j\right), \tag{10}$$

where $\mathbf{u} = (u_1, \cdots, u_d)^T$ is the displacement and ∂_{x_j} denotes the partial derivative operator along the j-th axis in the sense of distribution [21]. Note that $\varepsilon = (\varepsilon_{ij})_{d\times d}$ is the corresponding strain, i.e. the deformation [20].

The rest of this paper is organized as follows: In Section 2, we first introduce functions of bounded deformation, then propose our registration model by regularizing the displacement field to be a function of bounded deformation, then we prove that there exist solutions of the model. In Section 3, we first discretize our registration model, then we show some 2D and 3D numerical experiments and the corresponding results in two subsections, respectively. In Section 4, we draw some conclusion on our model and discussion on future work.

II. Bounded Deformation Registration Model

A. Pre-Knowledge of BD Functions

In this paper, we construct the registration model by supposing the displacement field $\mathbf{u}$ to be a function of bounded deformation. The space of functions of bounded deformation, denoted as $BD(\Omega)$, is defined as [19]:

$$BD(\Omega) := \Big\{\mathbf{u} \in L^1(\Omega;\mathbb{R}^d) \,\big|\, \varepsilon_{ij}(\mathbf{u}) = \frac{1}{2}(\partial_{x_i}u_j + \partial_{x_j}u_i) \ \text{ is a bounded measure}, 1 \le i, j \le d\Big\}, \tag{11}$$

provided that Ω is an open bounded subset of $\mathbb{R}^d$. The so-called bounded deformation of a function $\mathbf{u} \in L^1(\Omega;\mathbb{R}^d)$ is defined and denoted as [16]:

$$|\mathcal{E}(\mathbf{u})|(\Omega) := sup\Big\{\int_\Omega \sum_{i,j=1}^{d}\left(u_i\partial_{x_j}\phi_{ij} + u_j\partial_{x_i}\phi_{ij}\right)d\mathbf{x} \,\Big|\, \forall\boldsymbol{\phi} \in C_0^\infty(\Omega;\mathbb{R}^{d\times d}), \|\boldsymbol{\phi}\| \le 1\Big\}. \tag{12}$$

For every $\mathbf{u} \in BD(\Omega)$, $\mathcal{E}(\mathbf{u})$ is actually a Radon measure. By Radon-Nikodym decomposition theorem, we can decompose $\mathcal{E}(\mathbf{u})$ into the absolutely continuous part $\mathcal{E}^a(\mathbf{u})$ and the singular part $\mathcal{E}^s(\mathbf{u})$ with respect to Lebesgue measure $\mathcal{L}^n$, i.e. $\mathcal{E}(\mathbf{u}) = \mathcal{E}^a(\mathbf{u}) + \mathcal{E}^s(\mathbf{u})$ [21]. Note that when $\mathbf{u} \in C^1(\Omega;\mathbb{R}^d)$, the singular part vanishes. Thus we can integrate by parts and find that the bounded deformation turns into

$$\begin{aligned}|\mathcal{E}(\mathbf{u})|(\Omega) &= sup\Big\{\int_\Omega \left(\nabla\mathbf{u} + \nabla^T\mathbf{u}\right)\cdot\boldsymbol{\phi}\, d\mathbf{x} \,\Big|\, \forall\boldsymbol{\phi} \in C_0^\infty(\Omega;\mathbb{R}^{d\times d}), \|\boldsymbol{\phi}\| \le 1\Big\}\\ &= \int_\Omega \|\nabla\mathbf{u} + \nabla^T\mathbf{u}\| d\mathbf{x}.\end{aligned} \tag{13}$$

The notation ∇^T means that $\nabla^T\mathbf{u} = (\nabla\mathbf{u})^T$ and the dot $\cdot$ denotes the elementwise scalar production of matrices. The latter equation holds by taking $\boldsymbol{\phi} = \frac{\nabla\mathbf{u}+\nabla^T\mathbf{u}}{\|\nabla\mathbf{u}+\nabla^T\mathbf{u}\|}$, provided $\nabla\mathbf{u} + \nabla^T\mathbf{u} \neq \mathbf{0}$. It is trivial when $\nabla\mathbf{u} + \nabla^T\mathbf{u} = \mathbf{0}$. Obviously, there are several choices for the matrix norm used here. A typical one is the Frobenius norm, i.e. $\|\boldsymbol{\phi}(\boldsymbol{x})\|_F = \sqrt{\sum_{i,j}\left(\boldsymbol{\phi}_{ij}(\boldsymbol{x})\right)^2}$. In this paper, we use the Frobenius norm for our registration model.

Using the concept of bounded deformation, a more concise definition of $BD(\Omega)$ is

$$BD(\Omega) := \left\{\mathbf{u} \in L^1(\Omega;\mathbb{R}^d) \;\middle|\; |\mathcal{E}(\mathbf{u})|(\Omega) < \infty\right\}.$$

Remark 1: In fact, by definition $W^{1,2}(\Omega,\mathbb{R}^d) \subset \mathrm{BD}(\Omega)$ [16], [23], *and* $\mathrm{BV}(\Omega,\mathbb{R}^d) \subset \mathrm{BD}(\Omega)$ *(*[21, *Remark* 4.8 and *Example* 7.7]*), i.e.* $\mathrm{BD}(\Omega)$ *is a more general function space.*

In 1978, Strang *et al.* [18] connected *BD* functions with the displacement fields in perfect plasticity and showed that $BD(\Omega)$ is the correct admissible space in the underlying variational principle. There are many research results about *BD* functions [20]–[22]. It can be easily checked that the space $BD(\Omega)$ endowed with the norm $\|\mathbf{u}\|_{BD(\Omega)} := \|\mathbf{u}\|_{L^1(\Omega;\mathbb{R}^d)} + |\mathcal{E}(\mathbf{u})|(\Omega)$ is a Banach space. In particular, $|\mathcal{E}(\mathbf{u})|(\Omega)$ is a semi-norm. Besides, $C_0^\infty(\Omega;\mathbb{R}^d)$ is dense in $BD(\Omega)$. Below, we introduce several important conclusions as lemmas and refer [22] for details.

Lemma 1: Given a sequence $\{\boldsymbol{u}_j\}_{j=1}^\infty \subset BD(\Omega)$ *satisfying* $\sup_j \|\boldsymbol{u}_j\|_{\mathrm{BD}(\Omega)} < \infty$, *there exists a subsequence* $\{\boldsymbol{u}_{j_n}\}_{n=1}^\infty \subset \{\boldsymbol{u}_j\}_{j=1}^\infty$ *and* $\boldsymbol{u} \in BD(\Omega)$ *such that*

$$\boldsymbol{u}_{j_n} \to \boldsymbol{u} \ \text{ in } \ L^1(\Omega;\mathbb{R}^d) \ \text{ as } \ n \to \infty.$$

Furthermore, if

$$\left|\mathcal{E}(\boldsymbol{u}_{j_n})\right|(\Omega) \le C\ ,$$

where C is a positive constant, then the lower semi-continuity holds:

$$|\mathcal{E}(\boldsymbol{u})|(\Omega) \le \liminf_{n\to\infty}\left|\mathcal{E}(\boldsymbol{u}_{j_n})\right|(\Omega).$$

Lemma 2: **(I)** *There exists a linear, continuous and surjective trace operator*

$$tr : BD(\Omega) \to L^1(\partial\Omega; \mathbb{R}^d)$$

such that $tr(\boldsymbol{u}) = \boldsymbol{u}\big|_{\partial\Omega}$ *if* $\boldsymbol{u} \in BD(\Omega) \cap C(\bar{\Omega}; \mathbb{R}^d)$; **(II)** *There exists a constant* $C = C(\Omega)$ *such that for every* $\boldsymbol{u} \in BD(\Omega)$ *with* $tr(\boldsymbol{u}) = \boldsymbol{0}$,

$$\|\boldsymbol{u}\|_{L^1(\Omega;\mathbb{R}^d)} \le C\,|\mathcal{E}(\boldsymbol{u})|\,(\Omega).$$

B. Proposed Model

The space $BD(\Omega)$ was first introduced to solve the problems of plasticity [18]–[20] by supposing that displacement fields in plastic bodies are of bounded deformation. By elastoplasticity theory [15], symmetric distribution derivatives of the displacement field can capture the coupling between/among components of displacement fields accurately and effectively. Moreover, functions of bounded deformation allows discontinuity, just as plastic materials allow discontinuities and even breakages inside. Hence the space $BD(\Omega)$ can be naturally used for image registration if we consider the objects in images are plastic bodies. Therefore, in this paper we regularize the displacement field $\mathbf{u}$ to be a *BD* function.

Meanwhile, in order to ensure $\mathbf{x} + \mathbf{u}(\mathbf{x}) \in \Omega,\ \forall \mathbf{x} \in \Omega$, we simply assume that $\mathbf{u}$ has compact support in Ω. In this case, $tr(\mathbf{u}) = \mathbf{u}\big|_{\partial\Omega} = \mathbf{0}$. From **Lemma 2** we see that

$$\|\mathbf{u}\|_{BD(\Omega;\mathbb{R}^d)} = \|\mathbf{u}\|_{L^1(\Omega;\mathbb{R}^d)} + |\mathcal{E}(\mathbf{u})|\,(\Omega) \le \tilde{C}\,|\mathcal{E}(\mathbf{u})|\,(\Omega),$$

i.e., the *BD* norm will be controlled by the semi-norm. Hence we can use the semi-norm rather than the *BD* norm as the regularization term. Besides, in this paper *SSD* is chosen as the data term, since it is easy to compute and each pair of images to be registered are in the same modality.

Based on above assumptions and considerations, we propose the following optimization model for the deformable registration problem:

$$\min_{\mathbf{u}\in\mathcal{K}} E(\mathbf{u}) = SSD(\mathbf{u}) + \lambda\,|\mathcal{E}(\mathbf{u})|\,(\Omega), \tag{14}$$

where $\lambda > 0$ is a weighted parameter balancing the data term and the regularization term, and

$$\mathcal{K} = \left\{\mathbf{u} \in BD(\Omega) \;\middle|\; \mathbf{u}\big|_{\partial\Omega} = \mathbf{0}\right\} \tag{15}$$

is the admissible set. Note that $\mathcal{K}$ is dense in $BD(\Omega)$.

C. Existence of Solutions

Functional analysis methods are often used to prove the existence and uniqueness of solutions to many mathematical models and partial differential equation [24]–[27]. Note that we use the semi-norm rather than the *BD*-norm here in the model (14). The semi-norm is convex in $\mathbf{u}$, whereas the convexity of the data term $SSD(\mathbf{u})$ remains unknown. Thus the energy $E(\mathbf{u})$ lacks convexity and we can not analyze it using the classic convex functional theory. Fortunately, for our deformable registration model, $\mathbf{u} \in \mathcal{K}$ has bounded deformation and compact support in Ω, we can get desired results by adding just a few simple conditions on the images.

Theorem 1: Suppose that $\Omega \subset \mathbb{R}^d$ *is an open bounded set with Lipschitz boundary, the image functions* $R, M : \Omega \to \mathbb{R}$ *are uniformly bounded and continuous almost everywhere. There exists at least one solution of the registration model* (14) *in the admissible set* $\mathcal{K}$.

Proof: Note that the energy $E(\mathbf{u}) \ge 0$ in (14) for all the deformation fields $\mathbf{u} \in \mathcal{K}$. Thus we can find a minimizing sequence $\{\mathbf{u}_j\} \subset \mathcal{K}$ such that

$$\sup_j \left|\mathcal{E}(\mathbf{u}_j)\right|(\Omega) \le \sup_j E(\mathbf{u}_j) \le E(\mathbf{u}_1) < \infty.$$

By **Lemma 1** we can see that

$$\|\mathbf{u}_j\|_{L^1(\Omega;\mathbb{R}^d)} \le C\left|\mathcal{E}(\mathbf{u}_j)\right|(\Omega),$$

where $C = C(\Omega)$ is a constant. This implies that

$$\sup_j \|\mathbf{u}_j\|_{BD(\Omega)} = \sup_j \left\{\|\mathbf{u}_j\|_{L^1(\Omega;\mathbb{R}^d)} + \left|\mathcal{E}(\mathbf{u}_j)\right|(\Omega)\right\} < \infty.$$

Thus we can obtain a subsequence $\{\mathbf{u}_{j_n}\} \subset \{\mathbf{u}_j\}$ and $\hat{\mathbf{u}} \in \mathcal{K} \subset BD(\Omega)$ such that

$$\mathbf{u}_{j_n} \to \hat{\mathbf{u}} \ \ in \ \ L^1(\Omega;\mathbb{R}^d)\ (n \to \infty),$$
$$\text{and } \left|\mathcal{E}(\hat{\mathbf{u}})\right|(\Omega) \le \liminf_{n\to\infty} \left|\mathcal{E}(\mathbf{u}_{j_n})\right|(\Omega).$$

Recall that M, R are uniformly bounded and continuous a.e. in Ω, thus

$$\|M(\mathbf{x} + \hat{\mathbf{u}}(\mathbf{x})) - R(\mathbf{x})\|^2 = \lim_{n\to\infty} \|M(\mathbf{x} + \mathbf{u}_{j_n}(\mathbf{x})) - R(\mathbf{x})\|^2.$$

Finally, we can conclude that

$$\begin{aligned} E(\hat{\mathbf{u}}) &= \|M(\mathbf{x} + \hat{\mathbf{u}}(\mathbf{x})) - R(\mathbf{x})\|^2 + \lambda\left|\mathcal{E}(\hat{\mathbf{u}})\right|(\Omega) \\ &\le \lim_{n\to\infty} \|M(\mathbf{x}+\mathbf{u}_{j_n}(\mathbf{x})) - R(\mathbf{x})\|^2 + \lambda \liminf_{n\to\infty} \left|\mathcal{E}(\mathbf{u}_{j_n})\right|(\Omega) \\ &\le \liminf_{n\to\infty} \left\{\|M(\mathbf{x} + \mathbf{u}_{j_n}(\mathbf{x})) - R(\mathbf{x})\|^2 + \lambda\left|\mathcal{E}(\mathbf{u}_{j_n})\right|(\Omega)\right\} \\ &= \liminf_{n\to\infty} E(\mathbf{u}_{j_n}), \end{aligned}$$

which means $\hat{\mathbf{u}}$ is exactly a solution of the deformable registration problem (14). □

Remark 2: The above theorem only ensures the existence of solutions of the model, while the uniqueness of solution remains unknown because the energy $E(\boldsymbol{u})$ *lacks convexity. Note that this theorem holds for both large-displacement case and small-displacement case since there is no restriction on the magnitude of the displacement field. Of course,* $\boldsymbol{u}$ *should satisfy the restriction* $\boldsymbol{x} + \boldsymbol{u}(\boldsymbol{x}) \in \Omega, \forall \boldsymbol{x} \in \Omega$.

In fact, for a small enough displacement field, we can modify the data term to be convex by simply taking the first-order approximation of the typical Taylor's expansion of $M(\mathbf{x} + \mathbf{u}(\mathbf{x}))$ at $\mathbf{u}(\mathbf{x})$:

$$M(\mathbf{u}(\mathbf{x}) + \mathbf{x}) \approx M(\mathbf{x}) + \nabla M(\mathbf{x}) \cdot \mathbf{u}(\mathbf{x}), \tag{16}$$

where ∇ denotes the common gradient operator. In this case the energy in (14) turns into

$$E(\mathbf{u}) = \|M(\mathbf{x}) + \nabla M(\mathbf{x}) \cdot \mathbf{u}(\mathbf{x}) - R(\mathbf{x})\|^2 + \lambda\,|\mathcal{E}(\mathbf{u})|\,(\Omega). \tag{17}$$

Theorem 2: There exists a unique minimizer of the energy functional (17).

Proof: By **Theorem 1** we know that there exists a minimizer of the energy functional (17). In addition, it can be easily checked that the model (17) is strictly convex since the data term is strictly convex and the regularization term is convex. Therefore, the minimizer is unique. □

III. Numerical Implementation and Experiments

In this section we first calculate the Euler-Lagrange equations of BD model and its related gradient descent flow. Then we develop a finite difference discretization of these equations and present some 2D and 3D numerical examples and the corresponding analysis of registration results.

For convenience, hereafter we will use the norm notation $\|\mathcal{E}\mathbf{u}\|_1$ to substitute the semi-norm $|\mathcal{E}\mathbf{u}|(\Omega)$, i.e. $\|\mathcal{E}\mathbf{u}\|_1 = |\mathcal{E}\mathbf{u}|(\Omega)$. Thus the registration energy of BD model (14) can be written as:

$$\begin{aligned} E(\mathbf{u}) &= \|M(\mathbf{x}+\mathbf{u}(\mathbf{x})) - R(\mathbf{x})\|^2 + \lambda\|\mathcal{E}\mathbf{u}\|_1 \\ &= \|M(\mathbf{u}) - R\|^2 + \lambda\|\mathcal{E}\mathbf{u}\|_1. \end{aligned} \tag{18}$$

Then we can take an arbitrary test function $\boldsymbol{\eta} \in C_0^\infty(\Omega;\mathbb{R}^d)$ and sufficient small $t \in \mathbb{R}$ to compute the first-order variation of $E(\mathbf{u})$ as follows:

$$\begin{aligned} f(t) &= E(\mathbf{u}+t\boldsymbol{\eta}) \\ &= \|M(\mathbf{u}+t\boldsymbol{\eta}) - R\|^2 + \lambda\|\mathcal{E}(\mathbf{u}+t\boldsymbol{\eta})\|_1. \end{aligned}$$

By the variational principle, we have $\frac{df}{dt}\big|_{t=0} = 0$. This needs to compute the derivative,

$$\begin{aligned} \frac{df}{dt} &= 2\left(M(\mathbf{u}+t\boldsymbol{\eta}) - R\right)\left(\nabla M(\mathbf{u}+t\boldsymbol{\eta})\cdot\boldsymbol{\eta}\right) \\ &\quad + \lambda\frac{\mathcal{E}(\mathbf{u}+t\boldsymbol{\eta})}{\|\mathcal{E}(\mathbf{u}+t\boldsymbol{\eta})\|_1}\cdot\mathcal{E}\boldsymbol{\eta} \\ &= 2\left(M(\mathbf{u}+t\boldsymbol{\eta}) - R\right)\left(\nabla M(\mathbf{u}+t\boldsymbol{\eta})\cdot\boldsymbol{\eta}\right) \\ &\quad - 2\lambda div\left(\frac{\mathcal{E}(\mathbf{u}+t\boldsymbol{\eta})}{\|\mathcal{E}(\mathbf{u}+t\boldsymbol{\eta})\|_1}\right)\cdot\boldsymbol{\eta}. \end{aligned}$$

Note that the fact $\frac{d}{d\mathbf{x}}\|\mathbf{x}\|_1 = \begin{cases} \frac{\mathbf{x}}{\|\mathbf{x}\|_1}, & if\ \mathbf{x}\neq\mathbf{0} \\ \mathbf{0}, & if\ \mathbf{x}=\mathbf{0} \end{cases}$ is employed to obtain the above first equation. The notation *div* denotes the conventional divergence operator, which is the adjoint operator of $-\nabla$, i.e. $\langle A, \nabla B\rangle = \langle -divA, B\rangle$ for $A \in \mathbb{R}^{d\times d}, B \in \mathbb{R}^d$. Thus according to (13), $\langle A, \mathcal{E}\boldsymbol{\eta}\rangle = \langle A, \nabla\boldsymbol{\eta} + \nabla^T\boldsymbol{\eta}\rangle = \langle -2divA, \boldsymbol{\eta}\rangle$.

Let $t = 0$ and substitute it into the derivative, we have

$$0 = \left(M(\mathbf{u}) - R\right)\nabla M(\mathbf{u}) - \lambda div\left(\frac{\mathcal{E}\mathbf{u}}{\|\mathcal{E}\mathbf{u}\|_1}\right)\cdot\boldsymbol{\eta}.$$

Note that $\boldsymbol{\eta}$ is arbitrary and $C_0^\infty(\Omega;\mathbb{R}^d)$ is dense in $BD(\Omega)$, we finally obtain the Euler-Lagrange equation:

$$\left(M(\mathbf{u}) - R\right)\nabla M(\mathbf{u}) - \lambda div\left(\frac{\mathcal{E}\mathbf{u}}{\|\mathcal{E}\mathbf{u}\|_1}\right) = \mathbf{0}. \tag{19}$$

Therefore, the gradient descent flow of the energy functional is:

$$-\frac{\partial\mathbf{u}}{\partial t} = \left(M(\mathbf{u}) - R\right)\nabla M(\mathbf{u}) - \lambda div\left(\frac{\mathcal{E}\mathbf{u}}{\|\mathcal{E}\mathbf{u}\|_1}\right). \tag{20}$$

A. Finite Difference Discretization

We take the 2D case as an example to discretize the registration model (18) and the corresponding gradient descent flow (20). As to 3D cases, the discretization method is analogous.

Without causing any misunderstanding, in this subsection all the previous notations and symbols remain the same in spite of discrete settings. Note that bold letters denote vector or matrix-valued functions. The image grid is

$$\Omega = \{\mathbf{x}\in\Omega \mid \mathbf{x} = (i,j),\quad 1\le i\le m,\ 1\le j\le n\},$$

where (m,n) denote the number of rows and columns, respectively. Thus the images M, R are matrices and $M_{ij} = M(i,j), R_{ij} = R(i,j)$ represent the intensities at position $\mathbf{x} = (i,j)$.

In discretization settings, $\mathcal{E}\mathbf{u} = \nabla\mathbf{u} + \nabla^T\mathbf{u}$ and the gradient of $\mathbf{u}$ can be computed numerically as

$$\begin{aligned} (\nabla\mathbf{u})_{ij} &= \begin{pmatrix} \delta_1^+u_1 & \delta_2^+u_1 \\ \delta_1^+u_2 & \delta_2^+u_2 \end{pmatrix}_{ij} \\ &= \begin{pmatrix} u_1(i+1,j)-u_1(i,j) & u_1(i,j+1)-u_1(i,j) \\ u_2(i+1,j)-u_2(i,j) & u_2(i,j+1)-u_2(i,j) \end{pmatrix}, \end{aligned}$$

for all the interior point $(i,j)\in\Omega$ and the point on the left and top boundary ($j=0, i=0$ *resp.*). As to the right and bottom boundary of Ω($j=n, i=m$ *resp.*), we can simply take zeros or the values of the adjacent column or row, respectively. $\nabla\mathbf{u}$ is actually a three-dimensional matrix, so is $\nabla\mathbf{u}+\nabla^T\mathbf{u}$. Hence, we can compute elementwisely that

$$\begin{aligned} &\left(\nabla\mathbf{u}+\nabla^T\mathbf{u}\right)_{ij} \\ &= \begin{pmatrix} 2\delta_1^+u_1\delta_2^+u_1 + \delta_1^+u_2 & \\ \delta_2^+u_1 + \delta_1^+u_2 & 2\delta_2^+u_2 \end{pmatrix}_{ij}, \\ &\left(\|\nabla\mathbf{u}+\nabla^T\mathbf{u}\|_1\right)_{ij} \\ &= \sqrt{4*\left(\delta_1^+u_1\right)_{ij}^2 + 2*\left(\delta_2^+u_1+\delta_1^+u_2\right)_{ij}^2 + 4*\left(\delta_2^+u_2\right)_{ij}^2}, \\ &\left(\frac{\nabla\mathbf{u}+\nabla^T\mathbf{u}}{\|\nabla\mathbf{u}+\nabla^T\mathbf{u}\|_1}\right)_{ij} \\ &= \begin{cases} \dfrac{\left(\nabla\mathbf{u}+\nabla^T\mathbf{u}\right)_{ij}}{\left(\|\nabla\mathbf{u}+\nabla^T\mathbf{u}\|_1\right)_{ij}}, & if\ \nabla\mathbf{u}+\nabla^T\mathbf{u}\neq\mathbf{0} \\ \mathbf{0}, & if\ \nabla\mathbf{u}+\nabla^T\mathbf{u}=\mathbf{0} \end{cases}. \end{aligned}$$

As to the *div* operator, given a matrix-valued function

$$\begin{aligned} \boldsymbol{\phi} &= \begin{pmatrix} \phi_{11} & \eta_{12} \\ \phi_{21} & \phi_{22} \end{pmatrix} : \Omega \to \mathbb{R}^{2\times 2}, \\ (div\boldsymbol{\phi})_{ij} &= \left(\delta_1^+\phi_{11} + \delta_2^+\phi_{12}, \delta_1^+\phi_{21} + \delta_2^+\phi_{22}\right)_{ij}^T. \end{aligned}$$

So far, we discretize the space domain. Then we can simply discretize the time domain by $\partial\mathbf{u}/\partial t = \left(\mathbf{u}^{(t+1)} - \mathbf{u}^{(t)}\right)/\delta t$, where δt denotes the time step between the $t-th$ and $(t+1)-th$ time node, $\mathbf{u}^{(t)}$ and $\mathbf{u}^{(t+1)}$ denote the displacement fields at the t-th and $(t+1)$-th time node, respectively.

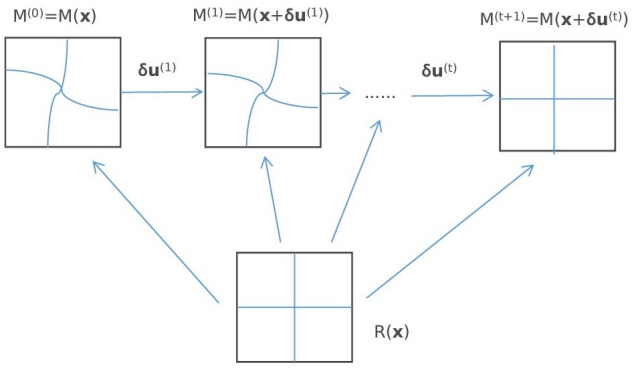

Fig. 1. Illustration of the registration process of BD model.

Therefore, we recall (20) and update the displacement field as follows:

$$\mathbf{u}^{(t+1)} = \mathbf{u}^{(t)} + \delta\mathbf{u}^{(t)},$$
$$\delta\mathbf{u}^{(t)} = \delta t\left\{\lambda div\left(\frac{\nabla\mathbf{u}+\nabla^T\mathbf{u}}{\|\nabla\mathbf{u}+\nabla^T\mathbf{u}\|_1}\right)^{(t)} - \left(M^{(t)}-R\right)\nabla M^{(t)}\right\},$$

where $M^{(t)}$ denotes the t-th registered moving image, which is obtained by interpolation, $M^{(t)}(\mathbf{x}) \leftarrow M^{(t-1)}(\mathbf{x}+\delta\mathbf{u}^{(t)})$ and pointwisely $\left(\nabla M^{(t)}\right)_{ij} = \left(\delta_1^+ M^{(t)}, \delta_2^+ M^{(t)}\right)^T$.

As we all know, the time step δt plays an important role in the gradient descent algorithm. In this paper it is adaptively chosen with inspiration from the implementation of demons-based algorithms [5], [6], [8]–[10]. Actually, in order to prevent the update of displacement field being too large, we set δt to be a matrix-valued parameter, which is pointwisely

$$(\delta t)_{ij} = \frac{1}{\left(M_{ij}^{(t)} - R_{ij}\right)^2 + \|\left(\nabla M^{(t)}\right)_{ij}\|^2}. \tag{21}$$

Whenever $(\delta t)_{ij} = \infty$, the update of the displacement field at the corresponding position (i, j) is zero at the current iteration and thus we can simply set $\delta\mathbf{u}_{ij}^{(t+1)} = 0$. As to the weight, it may take different values with specific registration tasks. In general, it is a good trial to start with $\lambda = 1/\delta t$, which is also a matrix-valued parameter and / here denotes the elementwise matrix division. This choice is mainly in order to counteract the possible bad effects of small time steps on the regularization term.

Ultimately, we present the following discrete gradient descent algorithm (see Fig. 1 for a brief illustration):

Step 1: Input the moving image M, fixed image R, maximum iteration, initialize $\delta\mathbf{u}^{(0)} = \mathbf{0}$, $M^{(0)} = M$, $t = 0$;

Step 2: calculate in turn $\nabla M^{(t)}$, $\nabla\mathbf{u}^{(t)}$, δt, $\delta\mathbf{u}^{(t)}$;

Step 3: update the displacement field as $\mathbf{u}^{(t+1)} = \mathbf{u}^{(t)} + \delta\mathbf{u}^{(t)}$;

Step 4: deform the moving image as $M^{(t+1)}(\mathbf{x}) \leftarrow M^{(t)}(\mathbf{x}+\delta\mathbf{u}^{(t+1)})$ by interpolation techniques such as linear and cubic interpolation;

Step 5: set $t = t+1$ and repeat **Step 2-4** until the maximum iteration is reached or other specific conditions are satisfied, such as $\|\delta\mathbf{u}^{(t)}\| < \varepsilon$ and $|E(\mathbf{u}^{(t+1)}) - E(\mathbf{u}^{(t)})| < \varepsilon$ for some appropriately given positive threshold ε.

Remark 3: As shown above, in the numerical algorithm there is no need for any smoothing of the displacement field or the update of the displacement field. Besides, we handle the singularity of the term $\frac{\nabla\mathbf{u}+\nabla^T\mathbf{u}}{\|\nabla\mathbf{u}+\nabla^T\mathbf{u}\|_1}$ effectively and efficiently. As to the interpolation step, we use the bilinear interpolation method in 2D cases and trilinear interpolation method in 3D cases for all numerical experiments in this paper.

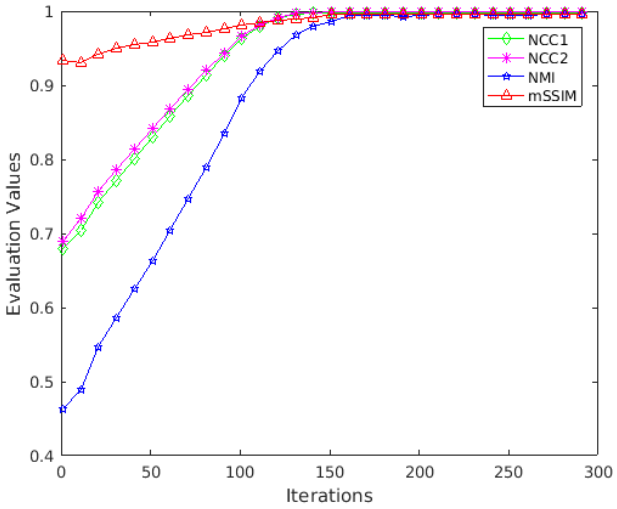

Fig. 2. The evaluation values of mSSIM, NCC1, NMI and NCC2 during the registration processing of BD model in the first experiment with synthetic images, see Fig. 3. After 150 iterations of processing, we can obtain a satisfactory result. Then the evaluation values remain nearly stable at a high level, which implies both the effectiveness of BD model and the stability of the gradient descent algorithm.

In the following two subsections we show some 2D and 3D numerical experiments. All these experiments are implemented using Matlab R2016 in a Ubuntu system, with an Intel Xeon E5-2650 CPU and 64GB memory. The above gradient descent algorithm is employed for solving out BD model in all 2D and 3D experiments. The Matlab codes are not optimized.

B. Registration Experiments and Results in 2D Cases

We demonstrate several experiments and compare BD model with Demons model (4), DiffeoDemons model (6) and VTV model (8) in this subsection. In order to compare different models, we need some unified, effective and convincing indicators to assess the quality of registration results of these models. In this paper we use the classical mean *SSIM* value [28], the normalized mutual information (*NMI*) [29], the normalized correlation coefficient (*NCC1*) and the normalized cross correlation (*NCC2*) to measure the similarity between images, where

$$NCC1(M,R) = \frac{\sum_i\sum_j(M_{ij}-\bar{M})(R_{ij}-\bar{R})}{\sqrt{\left(\sum_i\sum_j(M_{ij}-\bar{M})^2\right)\left(\sum_i\sum_j(R_{ij}-\bar{R})^2\right)}},$$
$$NCC2(M,R) = \frac{\sum_i\sum_j M_{ij}R_{ij}}{\sqrt{\left(\sum_i\sum_j M_{ij}^2\right)\left(\sum_i\sum_j R_{ij}^2\right)}},$$
$$\bar{M} = \frac{1}{|\Omega|}\sum_i\sum_j M_{ij}, \quad \bar{R} = \frac{1}{|\Omega|}\sum_i\sum_j R_{ij},$$

TABLE I
EVALUATION OF REGISTRATION MODELS BY $(mSSIM, NCC1, NMI, NCC2)^T$

Models \ Images	Synthetic	Hand	Brain	Liver
No DIR	0.9332	0.5392	0.7043	0.6229
	0.6949	0.8032	0.9220	0.8959
	0.4625	0.2975	0.4791	0.4508
	0.6957	0.8511	0.9371	0.8903
Demons [5], [6]	0.9783	0.8733	0.9718	0.8651
	0.9366	0.9778	0.9968	0.9898
	0.8360	0.6757	0.9043	0.8248
	0.9409	0.9854	0.9967	0.9893
DiffeoDemons [8]–[10]	0.9897	0.8241	0.9843	0.7971
	0.9732	0.9735	0.9981	0.9710
	0.8716	0.6673	0.9213	0.7291
	0.9740	0.9853	0.9968	0.9729
VTV [11], [12]	0.9869	0.8118	0.9757	0.7654
	0.9896	0.9564	0.9973	0.9520
	0.9470	0.6096	0.9364	0.6891
	0.9939	0.9786	0.9971	0.9523
proposed BD	**0.9975**	**0.9659**	**0.9864**	**0.9295**
	0.9999	**0.9942**	**0.9995**	**0.9959**
	0.9968	**0.7315**	**0.9528**	**0.9238**
	1.0000	**0.9965**	**0.9974**	**0.9970**

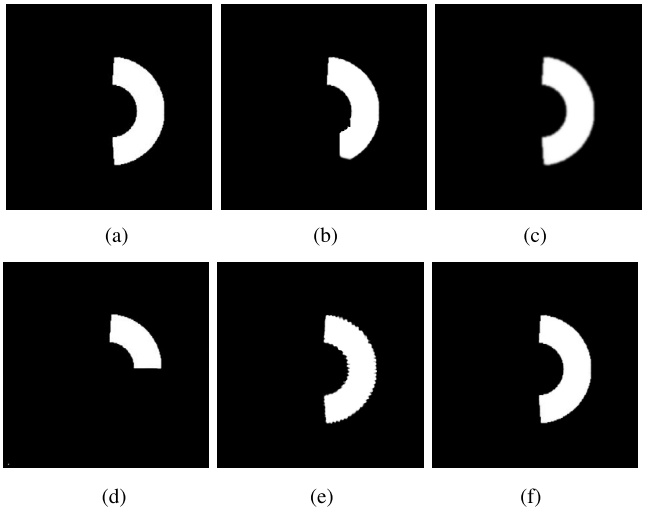

Fig. 3. Comparison of Demons, DiffeoDemons, VTV and BD models. The mean SSIM values of the moving image, Demons, DiffeoDemons, VTV and BD registration results with the fixed image are 0.9332, 0.9783, 0.9897, 0.9869, and 0.9975, respectively. (a) Fixed. (b) Demons. (c) DiffeoDemons. (d) Moving. (e) VTV. (f) BD.

and $|\Omega|$ denotes the number of pixels in image domain. These four values are all in the range of [0, 1], and the higher score, the better.

In all 2D numerical experiments, for BD model, we just adaptively set the time step as (21) and simply fixed the weight parameter $\lambda = 1.0/\delta t$. Besides, the gradient descent algorithm is quite stable. Usually after 150 iterations of processing, we can obtain a satisfactory result (See Fig. 2 for example). Then the result may get slightly better with the process going on and finally remains at a stable status. In this paper we run

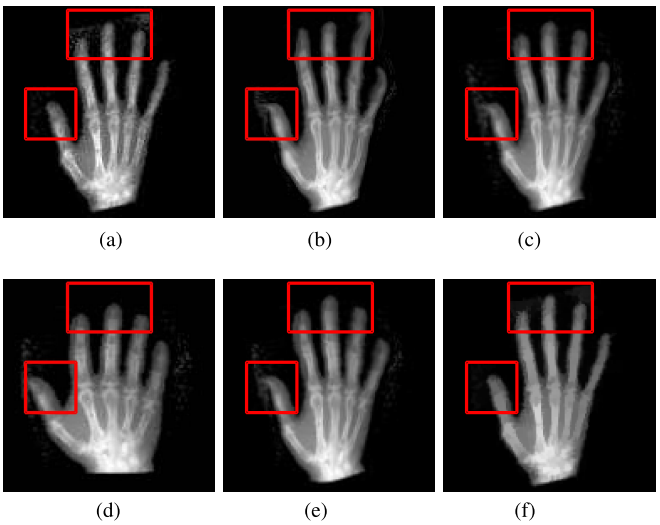

Fig. 4. Registration of X-ray images of hands. The mean SSIM values of the moving image, Demons, DiffeoDemons, VTV and BD registration results with the fixed image are 0.5392, 0.8733, 0.8241, 0.8118 and 0.9659, respectively. (a) Fixed. (b) Demons. (c) DiffeoDemons. (d) Moving. (e) VTV. (f) BD.

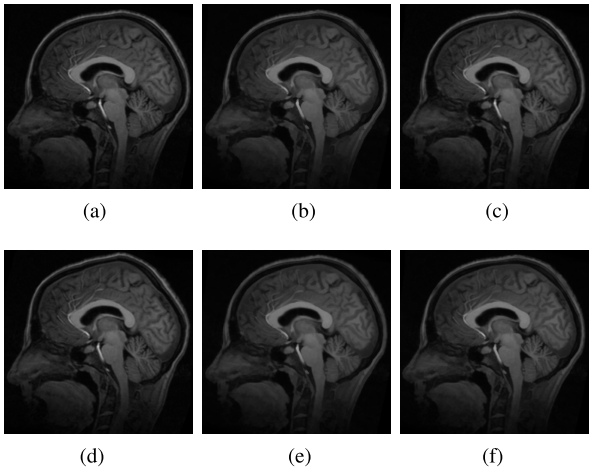

Fig. 5. Registration of MR brain images. The mean SSIM values of the moving image, Demons, DiffeoDemons, VTV and BD registration results with the fixed image are 0.7043, 0.9718, 0.9843, 0.9757 and 0.9864, respectively. (a) Fixed. (b) Demons. (c) DiffeoDemons. (d) Moving. (e) VTV. (f) BD.

BD model for 200 iterations in each 2D experiment to obtain the registered image since it appears sufficient for the *mSSIM* value to change less than 1.0×10^{-3}. One can also consider stopping the registration process when a specific similarity measure changes less than some threshold.

We choose the best result of each registration model for comparison. The evaluation results are in Table I. Note that the intensity values of images in these four experiments are all in the range of [0, 255]. In Table I we can see that BD model has the best performance in all four experiments. For each pair of test images, the evaluation values are arranged in a column in the order of *mSSIM*, *NCC1*, *NMI* and *NCC2*. This table confirms numerically that our bounded deformation regularization term is more suitable for the deformable image registration tasks than the bounded variation term and the L^2-norm terms.

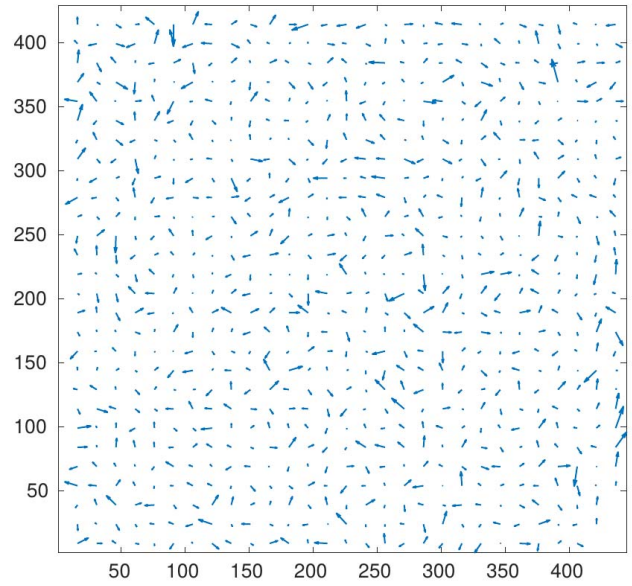

Fig. 6. The displacement field of brain images obtained by BD model. The lengths and directions of the arrows represent the magnitudes and directions of the displacement vectors at corresponding positions, respectively. The spacing is [15,15]. Considering the magnitudes and directions, BD model finds a discontinuous displacement field. As to displacement fields obtained by the other three models, we attach their figures in the supplementary file.

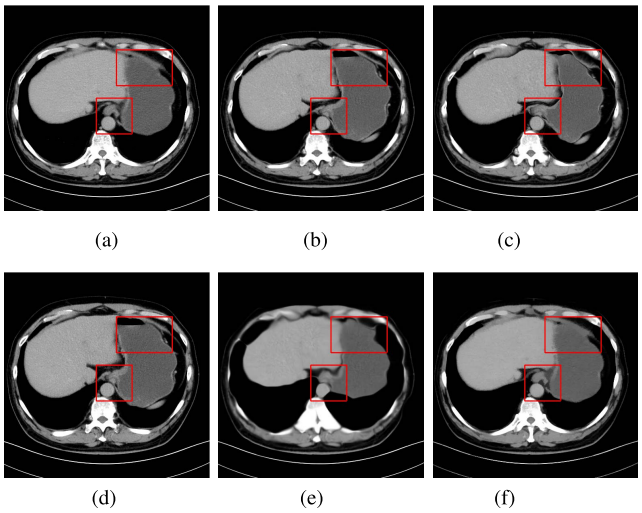

Fig. 7. Registration results of liver images. The mean SSIM values of the moving image, Demons, DiffeoDemons, VTV and BD registration results with the fixed image are 0.6229, 0.8651, 0.7971, 0.7654 and 0.9295, respectively. We can see that BD model effectively warps the moving image to the fixed image, especially in two red box-bounded regions. As to the corresponding zoomed-in images and displacement fields, see Fig. 8. (a) Fixed. (b) Demons. (c) DiffeoDemons. (d) Moving. (e) VTV. (f) BD.

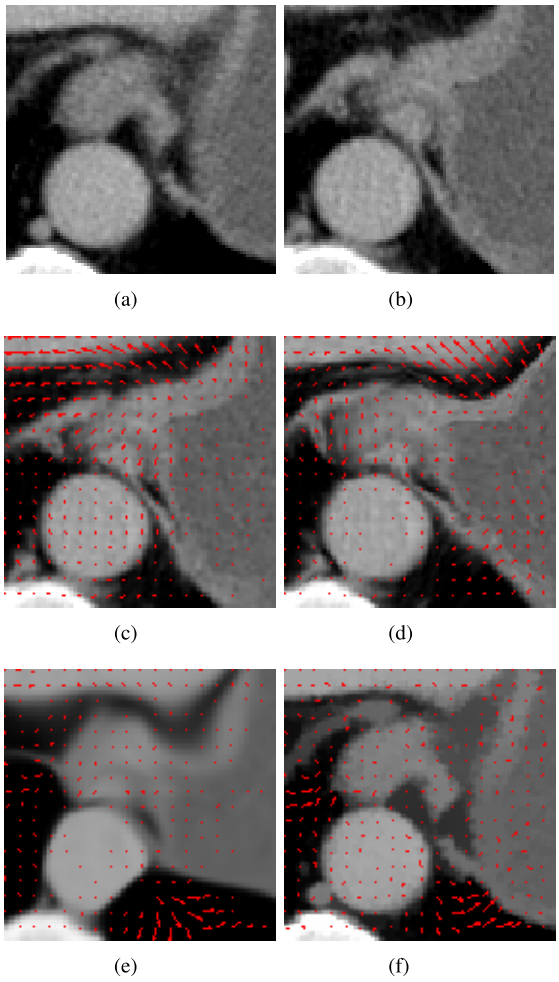

Fig. 8. Corresponding square areas of the images or registration results in Fig. 7. We can see that BD model achieves the best registration result, especially along the edges of the liver and in the right-sided liver region, VTV model just fails to register the gray circle centered in the area, which is the aorta. Demons and DiffeoDemons models fail to register the right-sided liver region. We can also see that Demons and DiffeoDemons models intend to obtain continuous and smooth displacement fields, whereas VTV and BD models obtain discontinuous displacement fields whose directions are inconsistent, especially in the upper-left and bottom-right parts of this area. Obviously the displacement field obtained by BD model is different from that obtained by VTV model. We observe that BD model performs better than VTV model according to the registered images of this specific area, Fig. 7 and Table I. The reason why BD model outperforms the other three models is that BD model searches solutions in a more general and more appropriate function space (***Remark* 1**). (a) Fixed. (b) Moving. (c) Demons. (d) DiffeoDemons. (e) VTV. (f) BD.

The first numerical experiment is to register a pair of synthetic images. The size of images is 308×308. We run the gradient descent algorithm of BD model for 200 iterations to obtain the registered image (Fig. 3), consuming 18.7903 seconds. The registration result of VTV model has obvious burrs on the edges. The registration result of DiffeoDemons model is oversmoothed and blurred. Demons model does not align the images very well, especially in the bottom region. This example shows that BD model can register images with sharp edges and large intensity changes.

In the second experiment we register two X-ray images of size 128×128 which are originally utilized in [11], see Fig. 4. The running time of 200 iterations of BD model is 9.2799 seconds. Note that the registration result of BD model is not only the one achieves the highest score, but also the most faithfully one that restores the details of the fixed image, especially in regions around the fingertips of the thumb, index and ring fingers. This example shows that the proposed BD model can register images with heavy noise.

TABLE II
EVALUATION OF REGISTRATION RESULTS ON 4D-CT DATABASE USING MEANTRE (STDTRE) VALUES

Models	Case1	Case2	Case3	Case4	Case5	Case6	Case7	Case8	Case9	Case10
cTVL1 [33]	0.78 (0.92)	0.78 (0.92)	0.93 (1.09)	1.24 (1.30)	1.22 (1.43)	0.94 (0.99)	1.01 (0.96)	1.11 (1.28)	0.98 (1.00)	0.94 (1.03)
cEPE [34]	0.80 (0.92)	0.77 (0.92)	0.92 (1.10)	1.22 (1.24)	1.21 (1.47)	0.90 (1.00)	0.98 (1.01)	1.16 (1.45)	1.00 (0.97)	0.99 (1.28)
NLR [35]	0.77 (0.90)	0.78 (0.89)	0.93 (1.06)	1.27 (1.26)	1.11 (1.46)	0.91 (1.00)	0.86 (0.98)	1.03 (1.19)	0.97 (0.94)	0.87 (0.97)
LMP [36]	**0.74** (0.90)	0.78 (0.90)	0.91 (1.05)	1.24 (1.25)	1.17 (1.48)	0.90 (1.00)	0.87 (0.97)	1.04 (1.18)	0.98 (0.96)	0.89 (0.99)
SGM3D [37]	0.76 (0.92)	**0.72** (**0.87**)	0.94 (1.07)	1.24 (1.26)	1.15 (1.42)	0.90 (0.98)	0.89 (0.95)	1.13 (1.40)	**0.91** (0.93)	0.83 (0.92)
NGF(a) [38]	0.78 (0.89)	0.79 (0.90)	0.93 (1.05)	1.27 (1.27)	**1.07** (1.46)	0.90 (0.99)	0.85 (0.98)	1.03 (1.23)	0.94 (0.93)	0.86 (0.97)
NGF(b) [38]	0.76 (0.89)	0.80 (0.88)	0.96 (1.07)	1.33 (1.29)	1.18 (1.45)	1.03 (1.04)	0.92 (0.93)	1.13 (**1.15**)	1.00 (0.96)	0.91 (0.99)
pTV [39]	0.79 (0.94)	0.74 (0.91)	0.95 (1.09)	**1.21** (**1.19**)	1.24 (1.50)	0.96 (1.01)	0.97 (0.99)	1.17 (1.47)	1.03 (1.08)	1.00 (1.02)
isoPTV [12]	0.76 (0.90)	0.77 (0.89)	0.90 (1.05)	1.24 (1.29)	1.12 (1.44)	0.85 (**0.89**)	0.80 (1.28)	1.34 (1.93)	0.92 (0.94)	**0.82** (**0.89**)
pTVreg [12]	0.80 (0.89)	0.77 (0.90)	0.92 (1.07)	1.30 (1.27)	1.13 (1.42)	**0.78** (0.92)	0.79 (0.91)	**1.00** (1.29)	**0.91** (0.95)	0.82 (0.97)
proposed BD	0.78 (**0.86**)	0.78 (0.90)	**0.90** (**1.04**)	1.23 (1.28)	1.16 (**1.34**)	0.88 (0.95)	**0.76** (**0.81**)	1.02 (1.22)	0.96 (**0.90**)	0.85 (0.95)
No DIR	4.01 (2.91)	4.65 (4.09)	6.73 (4.21)	9.42 (4.81)	7.10 (5.15)	11.10 (6.98)	11.59 (7.87)	15.16 (9.11)	7.82 (3.99)	7.63 (6.54)

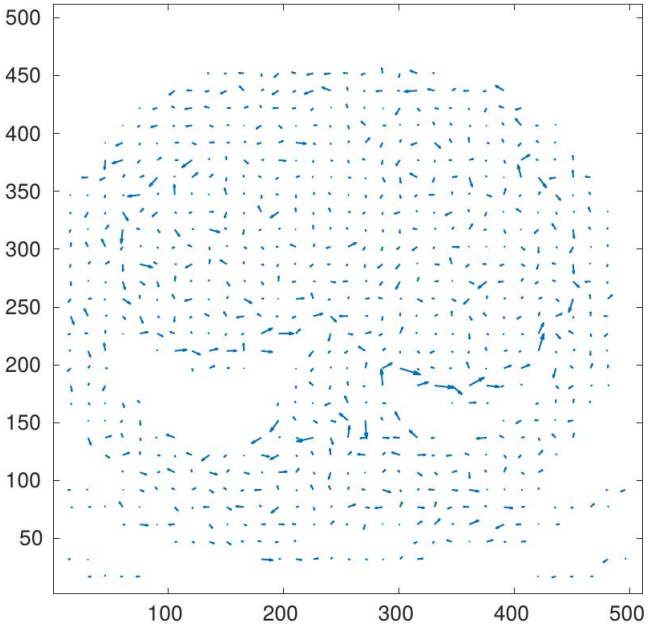

Fig. 9. The displacement field of liver images obtained by BD model. The lengths and directions of the arrows represent the magnitudes and directions of the displacement vectors at corresponding positions, respectively. The spacing is [15,15]. Considering the magnitudes and directions of vectors, BD model obtains a discontinuous displacement field. As to displacement fields obtained by the other three models, we attach their figures in the supplementary file.

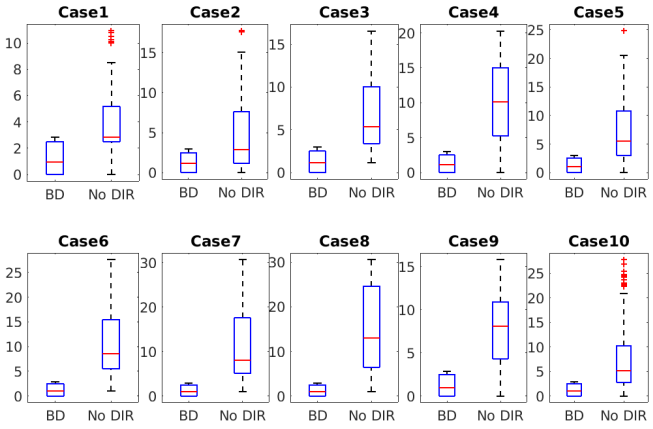

Fig. 10. Evaluation of the registration error on the whole 4D-CT database using the TRE indicator in millimeter. We can see that the BD model significantly reduces the registration error of corresponding landmarks for each case.

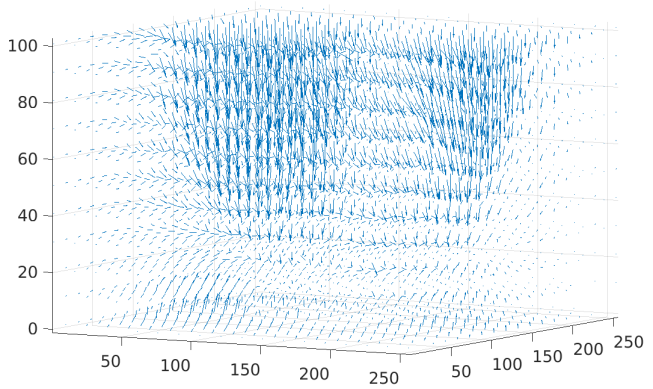

Fig. 11. The displacement field of Case 3 of 4D-CT database obtained by BD model. The spacing along x,y,z-axes is [15,15,10]. Displacement vectors located within the lungs are obviously denser, with larger magnitudes than those located outside the lungs. Besides, along the lung/chest wall, the directions of displacement vectors are obviously inconsistent or even opposite. Thus BD model obtains a discontinuous displacement field. We attach a more detailed figure in the supplementary file.

In the third experiment we register two MR images of brain whose sizes are 429×442. The running time of 200 iterations of BD model is 21.9962 seconds. All four models obtain satisfactory results, among which the result of BD model is slightly better, see Fig. 5 and Table I. The displacement fields obtained by Demons and DiffeoDemons models are continuous, whereas the displacement fields obtained by VTV and BD models are discontinuous. See Fig. 6 for the displacement field obtained by BD model, and the supplementary file for displacement fields obtained by the other three models.

In the last 2D experiment, we demonstrate the registration results of two CT images of liver of the same patient, see Fig. 7. The image size is 512×512 and the running time of 200 iterations of BD model is 24.3545 seconds. Medical images often contain a variety of intensity inhomogeneity and thus the contrasts are very low, just like the ones here. We can see that the result of BD model not only gains

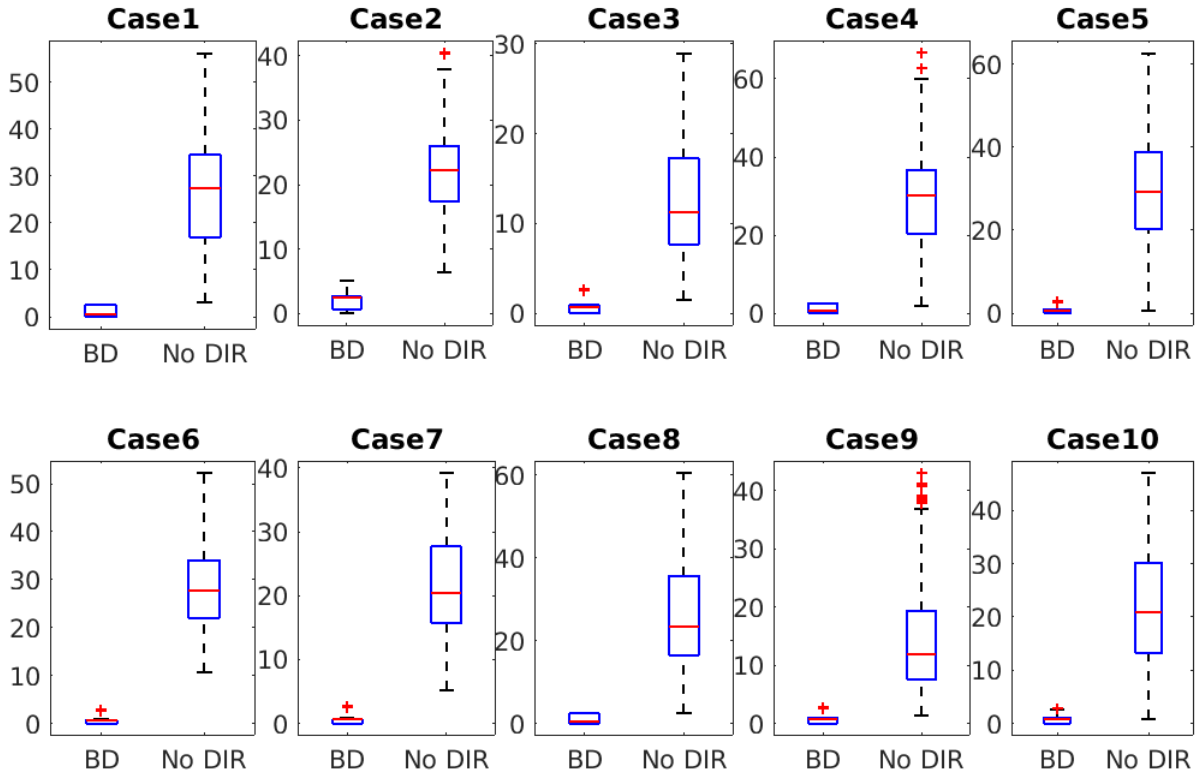

Fig. 12. Evaluation of the registration error on the whole COPD database using the TRE indicator in millimeter. We can see that BD model significantly reduces the registration error of corresponding landmarks for each case.

the highest similarity scores, but also is the first-rate to preserve the edges in the moving image. This example shows the ability of the proposed model to register intensity inhomogeneity and to preserve the discontinuity of edges, see Fig. 8, Fig. 9. For detailed figures of displacement fields obtained by Demons, DiffeoDemons, VTV and BD models, we refer to the supplementary file.

C. Registration Experiments and Results in 3D Cases

In this subsection, we evaluate BD model on two public 3D abdominal lung CT time-series databases,[1] namely DIR COPDgene and 4D-CT databases. Both databases have manually annotated landmarks. The target registration error (TRE) is defined as the Euclidean distance between two corresponding landmarks. The mean the standard of TRE values are used to summarize the registration accuracy. To keep the evaluation methodology in accordance with the literature, we used the snap-to-voxel TRE evaluation strategy (the landmark position from the registration is snapped to the nearest voxel center) for these two databases.

4D-CT database [30], [31] consists of 10 different cases and each case consists of 10 sequences. The former 5 cases have an average voxel resolution of $1.1\,mm \times 1.1\,mm \times 2.5\,mm$ and an average image size of $256 \times 256 \times 103$ voxels. The latter 5 cases have an average voxel resolution of $0.97\,mm \times 0.97\,mm \times 2.5\,mm$ and an average image size of $512 \times 512 \times 128$ voxels (see the webpage[2] for more details).

[1] https://www.dir-lab.com
[2] https://www.dir-lab.com/ReferenceData.html

For this database the average TRE is calculated for 300 anatomical landmarks between two 3D sequences of extreme inhale and exhale phases, with the exhale phase image as the fixed and the inhale phase image as the moving image. Note that the intensity values of images in this database varies in the range of $[0, 4000]$. We normalize them to be $[0, 1]$ in order to reduce the influence of possible sharp changes of intensity distribution between the extreme inhale/exhale phases. The time step δt of the gradient descent algorithm of BD model is adaptively chosen in (21). As to the weight parameter in BD model (18), it is set to be $1.0/\delta t$ for the former five cases and $2.0/\delta t$ for the latter five cases. The average running time of BD model for 200 iterations is 843.9074 seconds for the former five cases and 4.6173e+03 seconds for the latter five cases.

The evaluation of BD model on the whole 4D-CT database is shown in Fig. 10. From this boxplot figure, we can see that *BD* model significantly reduces the physical distance between corresponding landmarks. Note that when implementing BD model numerically and calculating the TRE values, the voxel resolution of image sequences should be considered and used. For each case, there are 300 landmarks that have been manually aligned. For $i-th$ moving landmark $\mathbf{x}_m^i = (x_m, y_m, z_m)$, we compute the displacement at it as $\mathbf{u}^i = (u_x, u_y, u_z)$, then TRE of the $i-th$ pair of landmarks is calculated as:

$$TRE(i) = \|\mathbf{res} \cdot \left(\mathbf{x}_m^i + \mathbf{u}^i - \mathbf{x}_f^i\right)\|_{L^2}, \tag{22}$$

where $\mathbf{x}_f^i = (x_f, y_f, z_f)$ is the voxel position of the $i-th$ fixed landmark and $\mathbf{res} = (rex_x, res_y, res_z)$ denotes the voxel

TABLE III
EVALUATION OF REGISTRATION RESULTS ON COPDgene DATABASE USING meanTRE (stdTRE) VALUES

Model	Case1	Case2	Case3	Case4	Case5
NLR [35]	1.33 (1.55)	2.34 (2.88)	1.12 (1.07)	1.54 (1.61)	1.39 (1.38)
LMP [36]	1.21 (1.46)	1.97 (2.38)	1.06 (0.96)	1.64 (1.75)	1.46 (1.45)
MILO [40]	0.93 (0.92)	1.77 (1.92)	0.99 (0.91)	1.14 (1.04)	1.02 (1.23)
SGM3D [37]	1.22 (2.73)	2.48 (3.79)	1.01 (0.93)	2.42 (3.56)	1.93 (3.24)
MRF [41]	1.00 (0.93)	1.62 (1.78)	1.00 (1.06)	1.08 (1.05)	0.96 (1.13)
meLDDMM [42]	0.90 (0.93)	1.56 (1.67)	1.03 (0.99)	0.94 (0.98)	0.85 (0.90)
isoPTV [12]	0.77 (**0.75**)	2.22 (2.94)	0.82 (0.80)	0.85 (0.86)	0.77 (0.84)
DIS-CO [43]	0.79 (0.85)	**1.46** (2.28)	0.84 (0.82)	0.74 (0.86)	0.71 (0.83)
pTVreg [12]	**0.71** (0.81)	1.89 (3.63)	0.77 (0.77)	**0.68** (**0.74**)	0.71 (0.83)
proposed BD	0.78 (0.89)	1.50 (**1.60**)	**0.76** (**0.72**)	0.79 (0.82)	**0.70** (**0.80**)
No DIR	25.90 (11.57)	21.77 (6.46)	12.29 (6.39)	30.90 (13.49)	30.90 (14.05)
Model	Case6	Case7	Case8	Case9	Case10
NLR [35]	2.08 (3.01)	1.10 (1.28)	1.57 (2.08)	0.99 (1.29)	1.42 (1.44)
LMP [36]	1.34 (1.65)	1.16 (1.46)	1.54 (2.25)	0.99 (1.32)	1.39 (1.46)
MILO [40]	0.99 (1.08)	1.03 (1.08)	1.31 (1.76)	0.86 (1.06)	1.23 (1.27)
SGM3D [37]	1.45 (2.42)	1.05 (1.43)	1.16 (1.79)	0.81 (0.67)	1.28 (1.29)
MRF [41]	1.01 (1.25)	1.05 (1.07)	1.08 (1.24)	0.79 (0.80)	1.18 (1.31)
meLDDMM [42]	0.94 (1.12)	0.94 (1.25)	1.12 (1.56)	0.88 (0.98)	1.17 (1.28)
isoPTV [12]	0.86 (1.92)	0.74 (1.06)	0.81 (1.84)	0.83 (1.22)	0.92 (0.85)
DIS-CO [43]	**0.64** (**0.80**)	0.79 (**0.85**)	**0.77** (**0.87**)	**0.62** (**0.66**)	0.86 (0.88)
pTVreg [12]	0.66 (1.15)	0.75 (0.87)	0.78 (1.61)	0.63 (1.01)	0.85 (0.86)
proposed BD	0.76 (1.10)	**0.72** (0.97)	0.82 (1.24)	0.71 (0.78)	**0.78** (**0.82**)
No DIR	28.32 (9.20)	21.66 (7.66)	25.57 (13.61)	14.84 (10.01)	22.48 (10.64)

resolution of the corresponding image sequence. We also show the displacement field of Case 3 of 4D-CT database in Fig. 11, which is not continuous at the lung/chest wall.

The comparison with state-of-the-art registration results, which are reported on the webpage,[3] is shown in Table II. The mean TRE value and the standard variation are computed for each case, and presented in the table as $meanTRE(stdTRE)$. The best values are in bold. Among all 20 competitions, BD model wins for 7 times. For the rest 13 values, our results are also in top 5.

The COPDgene study [32] provides 3D breath-hold CT lung images. It consists of 10 cases, each case including a pair of images at end-inhale and end-exhale, together with 300 publicly available landmarks per image. The average voxel resolution is $0.6\,mm \times 0.6\,mm \times 2.5\,mm$ and the average image size is $512 \times 512 \times 120$. For more details, we refer the webpage.[2] The exhale phase image is regarded as the fixed and the inhale phase image as the moving image. The time step δt of the gradient descent algorithm of BD model is adaptively chosen in (21). As to the weight parameter in BD model (18), it is set to be $2.0/\delta t$. The average running time of BD model for 200 iterations for these 10 cases is 4.0710e+03 seconds.

The evaluation of BD model on the whole COPDgene database is shown in Fig. 12. From this boxplot figure, we see that BD model significantly reduces the physical distance between corresponding landmarks. Note also that the voxel resolution of image sequences should be considered and used while implementing the BD model numerically and calculating the TRE values. The intensity values of images in this database also varies in the range of $[0, 4000]$ and we normalize them to be $[0, 1]$ as we do to 4D-CT database. We also show the displacement field of Case 10 of COPDgene database in Fig. 13, which is not continuous at the lung/chest wall.

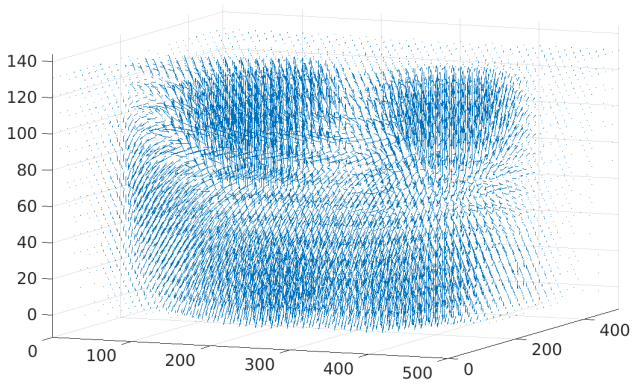

Fig. 13. The displacement field of Case 10 of COPDgene database obtained by BD model. The spacing along x,y,z-axes is [20,20,10]. We can see that displacement vectors located within the lungs are obviously denser, with larger magnitudes than those located outside the lungs. Besides, along the lung/chest wall, the directions of displacement vectors are obviously inconsistent or even opposite. Hence we know that the displacement field is discontinuous. We attach a more detailed figure in the supplementary file.

The comparison with state-of-the-art registration results, which are reported on the webpage[3], is shown in Table III. The mean TRE value and the standard variation are computed for each case, and presented in the table as $meanTRE(stdTRE)$. The best values are in bold. Among all 20 competitions, BD model wins for 8 times. For the rest 12 values, our results are also in the top 5.

[3]https://www.dir-lab.com/Results.html

IV. Conclusion and Discussion

In this paper, we proposed a novel variational model (14) for image registration problem by regularizing the displacement field as a *BD* function. Based on good properties of the space $BD(\Omega)$, we prove the existence of solutions of BD model. Furthermore, with small displacement assumption the solution is unique. We derive the gradient descent flow of BD model and then discretize the corresponding partial differential equations. An adaptive time step is chosen and is proved to be effective later in the numerical experiments. In four 2D experiments, BD model achieves the best registration results among three other classical and state-of-the-art models, showing the ability of BD model of handling both continuous and discontinuous displacement fields in images. Moreover, in 3D experiments implemented on two public databases, BD model obtains satisfactory registered results. These results are competitive when comparing with other state-of-the-art methods. To summarize, we conclude that BD model is an effective deformable registration model and *BD* functions are appropriate choices for describing displacement fields in images.

Most existing registration methods, which are not necessarily in the variational framework, can only deal with continuous and smooth displacement fields [1]–[3], for instance, Free-Form Deformation model [45], Kernel Functions-Based model [46], Demons and Diffeomorphic Demons models we mentioned above. VTV model (8) can tackle non-smooth displacement fields, in which the regularization term was firstly proposed and used for color image denoising [11]. BD model (18) is inspired by the theory of elastoplasticity and thus has a clear physical meaning of dealing with both continuous and discontinuous displacement fields [15]. Actually, from the view of elastoplasticity, the space of *BD* functions is a more suitable setting for describing displacement fields that may be discontinuous, and the symmetric distribution derivatives of a displacement field can capture the coupling between/among its components properly and effectively [15], [21]. Although VTV model also involves a kind of coupling with respect to distribution derivatives of the displacement fields, that coupling is much weaker since it only occurs in the diffusion coefficients in the Euler-Lagrange equation of the VTV energy functional [11]. Moreover, let $BV(\Omega, \mathbb{R}^d)$ be the space of vector-valued functions of bounded variation (corresponding to VTV model) and $BD(\Omega)$ be the space of functions of bounded deformation, then $BV(\Omega, \mathbb{R}^d)$ is a strict subspace of $BD(\Omega)$ (See [21, *Remark* 4.8 and *Example* 7.7]). This implies that when we search a minimizer of VTV model, we will get a displacement field that is of bounded deformation. However, when we minimize the registration energy based on the *BD* regularization term rather than the VTV regularization term, we can find more appropriate displacement fields which may not belong to $BV(\Omega, \mathbb{R}^d)$ since we search solutions in a more general and much bigger function space. 2D and 3D numerical experiments show that BD model indeed finds better displacement fields and thus performs better than VTV model.

The data term in the registration model, also known as (dis)similarity measure between images, has many other choices [2], [3]. We choose *SSD* term in this paper for two reasons. One is that the images in this paper are of the same modality, the other is that *SSD* is easy to understand and compute. Notably, in 3D numerical experiments, BD model does not win all cases. There are two reasons for this. Firstly, *SSD* only contains the intensity information and is possibly not the best choice for a registration data term even though the images to be registered are of the same modality [44]. Secondly, for each 3D database, we use a set of fixed parameters for all instances. BD model may obtain slightly better performance by replacing *SSD* with more appropriate data terms or by tuning the parameters separately for each 3D instance. We will try both ways in our future work.

In addition, we will try to register images of different modalities in future work and thus a more suitable data term is needed. At present there are several options for that, such as *LCC* [12] and *NMI* [29]. Besides, when implementing the numerical experiments we find that sometimes different interpolation methods may influence the registration results while sometimes may not. This is worth considering in future work. Fortunately, for most cases we encounter, bilinear or trilinear interpolation is enough.

At last, a fast and adaptive numerical algorithm is a key point in future work since registration tasks often involve a large amount of computations. Deep learning techniques have caused and will continue to cause changes in both ideas and methods in various fields of image processing and analysis [47], [48]. With deep learning techniques [49]–[52], images may be registered in a single shot in very short time using a pre-trained deep network. However, these deep learning techniques are currently limited by the need of large amounts of image pairs that have been accurately registered and the large amount of computational ability for training the registered images. Besides, the registration results of these deep learning techniques are not much better than those obtained by variational models [49], sometimes may even be worse [50], [51]. In a word, variational deformable registration models are still effective and competitive in the foreseeable future.

Acknowledgment

The authors highly appreciate the anonymous reviewers for giving thoughtful suggestions and comments which are very helpful to improve the paper. They also would like to thank the multidisciplinary team of liver, biliary and pancreatic tumors in Nanjing Drum Tower Hospital, China for providing the CT images of liver used in the last 2D numerical experiment.

References

[1] A. Sotiras, C. Davatzikos, and N. Paragios, "Deformable medical image registration: A survey," *IEEE Trans. Med. Imag.*, vol. 32, no. 7, pp. 1153–1190, Jul. 2013.

[2] J. Modersitzki, *FAIR: Flexible Algorithms for Image Registration*, vol. 6. Philadelphia, PA, USA: SIAM, 2009.

[3] L. G. Brown, "A survey of image registration techniques," *ACM Comput. Surv.*, vol. 24, no. 4, pp. 325–376, Dec. 1992.

[4] C. Broit, "Optimal registration of deformed images," Ph.D. dissertation, Dept. Comput. Inf. Sci., Univ. Pennsylvania, Philadelphia, PA, USA, 1981.

[5] J.-P. Thirion, "Image matching as a diffusion process: An analogy with Maxwell's demons," *Med. Image Anal.*, vol. 2, no. 3, pp. 243–260, 1998.

[6] D.-J. Kroon and C. H. Slump, "MRI modalitiy transformation in demon registration," in *Proc. IEEE Int. Symp. Biomed. Imag., Nano Macro (ISBI)*, Jun./Jul. 2009, pp. 963–966.

[7] S. Haker, L. Zhu, A. Tannenbaum, and S. Angenent, "Optimal mass transport for registration and warping," *Int. J. Comput. Vis.*, vol. 60, no. 3, pp. 225–240, 2004.

[8] T. Vercauteren, X. Pennec, A. Perchant, and N. Ayache, "Symmetric log-domain diffeomorphic registration: A demons-based approach," in *Proc. MICCAI*. Berlin, Germany: Springer, 2008, pp. 754–761.

[9] T. Vercauteren, X. Pennec, A. Perchant, and N. Ayache, "Diffeomorphic demons: Efficient non-parametric image registration," *NeuroImage*, vol. 45, no. 1, pp. S61–S72, 2009.

[10] H. Lombaert, L. Grady, X. Pennec, N. Ayache, and F. Cheriet, "Spectral log-demons: Diffeomorphic image registration with very large deformations," *Int. J. Comput. Vis.*, vol. 107, no. 3, pp. 254–271, 2014.

[11] N. Chumchob, "Vectorial total variation-based regularization for variational image registration," *IEEE Trans. Image Process.*, vol. 22, no. 11, pp. 4551–4559, Nov. 2013.

[12] V. Vishnevskiy, T. Gass, G. Szekely, C. Tanner, and O. Goksel, "Isotropic total variation regularization of displacements in parametric image registration," *IEEE Trans. Med. Imag.*, vol. 36, no. 2, pp. 385–395, Feb. 2017.

[13] A. Bartoli, "Groupwise geometric and photometric direct image registration," *IEEE Trans. Pattern Anal. Mach. Intell.*, vol. 30, no. 12, pp. 2098–2108, Dec. 2008.

[14] B. Chen *et al.*, "Color image analysis by quaternion-type moments," *J. Math. Imag. Vis.*, vol. 51, no. 1, pp. 124–144, 2015

[15] K. Washizu, *Variational Methods in Elasticity and Plasticity* (International Series of Monographs in Aeronautics and Astronautics), 2nd ed. New York, NY, USA: Pergamon Press, 1975.

[16] F. Lin and X. Yang, *Geometric Measure Theory-An Introduction*. Boston, MA, USA: International Press, 2002.

[17] B. Goldluecke, E. Strekalovskiy, and D. Cremers, "The natural vectorial total variation which arises from geometric measure theory," *SIAM J. Imag. Sci.*, vol. 5, no. 2, pp. 537–563, 2012.

[18] G. Strang, H. Matthies, and R. Temam, "Mathematical and computational methods in plasticity," in *Proc. Variational Methods Mech. Solids*, 1980, pp. 20–28.

[19] H. M. G. Strang and E. Christiansen, *The Saddle Point of a Differential Program*. New York, NY, USA: Wiley, 1979.

[20] R. Temam and G. Strang, "Functions of bounded deformation," *Arch. Rational Mech. Anal.*, vol. 75, no. 1, pp. 7–21, 1980.

[21] L. Ambrosio, A. Coscia, and G. D. Maso, "Fine properties of functions with bounded deformation," *Arch. Rational Mech. Anal.*, vol. 139, no. 3, pp. 201–238, 1997.

[22] A. C. Barroso, I. Fonseca, and R. Toadfr, "A relaxation theorem in the space of functions of bounded deformation," *Annali della Scuola Normale Superiore di Pisa-Classe di Scienze*, vol. 29, no. 1, pp. 19–50, 2000.

[23] L. C. Evans, *Partial Differential Equations*, 2nd ed. Providence, RI, USA: AMS, 2010.

[24] X. Lin and Z. Zhao, "Existence and uniqueness of symmetric positive solutions of 2n-order nonlinear singular boundary value problems," *Appl. Math. Lett.*, vol. 26, no. 7, pp. 692–698, 2013.

[25] F. Li and Y. Bao, "Uniform stability of the solution for a memory-type elasticity system with nonhomogeneous boundary control condition," *J. Dyn. Control Syst.*, vol. 23, no. 2, pp. 301–315, 2017.

[26] L. Liu, H. Li, C. Liu, and Y. Wu, " Existence and uniqueness of positive solutions for singular fractional differential systems with coupled integral boundary conditions," *J. Nonlinear Sci. Appl.*, vol. 10, no. 1, pp. 243–262, 2017.

[27] X.-N. Ma, P.-H. Wang, and W. Wei, "Constant mean curvature surfaces and mean curvature flow with non-zero Neumann boundary conditions on strictly convex domains," *J. Funct. Anal.*, vol. 274, no. 1, pp. 252–277, 2018.

[28] Z. Wang, A. C. Bovik, H. R. Sheikh, and E. P. Simoncelli, "Image quality assessment: From error visibility to structural similarity," *IEEE Trans. Image Process.*, vol. 13, no. 4, pp. 600–612, Apr. 2004.

[29] M. Hossny, S. Nahavandi, and D. Creighton, "Comments on 'information measure for performance of image fusion,"' *Electron. Lett.*, vol. 44, no. 18, pp. 1066–1067, Aug. 2008.

[30] R. Castillo *et al.*, "A framework for evaluation of deformable image registration spatial accuracy using large landmark point sets," *Phys. Med. Biol.*, vol. 54, no. 7, pp. 1849–1870, 2009.

[31] E. Castillo, R. Castillo, J. Martinez, M. Shenoy, and T. Guerrero, "Four-dimensional deformable image registration using trajectory modeling," *Phys. Med. Biol.*, vol. 55, no. 1, pp. 305–327, 2010.

[32] R. Castillo *et al.*, "A reference dataset for deformable image registration spatial accuracy evaluation using the COPDgene study archive," *Phys. Med. Biol.*, vol. 58, no. 9, pp. 2861–2877, 2013.

[33] S. Hermann and R. Werner, "TV-L1-based 3D medical image registration with the census cost function," in *Proc. Pacific-Rim Symp. Image Video Technol.* Berlin, Germany: Springer, 2013.

[34] S. Hermann and R. Werner, "High accuracy optical flow for 3D medical image registration using the census cost function," in *Image and Video Technology*, vol. 8333. Berlin, Germany: Springer, 2014, pp. 23–35.

[35] J. Rühaak, S. Heldmann, T. Kipshagen, and B. Fischer, "Highly accurate fast lung CT registration," *Proc. SPIE*, vol. 8669, Mar. 2013, Art. no. 86690Y.

[36] T. Polzin *et al.*, "Combining automatic landmark detection and variational methods for lung CT registration," in *Proc. 5th Int. Workshop Pulmonary Image Anal.*, 2013, pp. 85–96.

[37] S. Hermann, "Evaluation of scan-line optimization for 3D medical image registration," in *Proc. IEEE Conf. Comput. Vis. Pattern Recognit. (CVPR)*, Jun. 2014, pp. 3073–3080.

[38] L. König and J. Rühaak, "A fast and accurate parallel algorithm for non-linear image registration using normalized gradient fields," in *Proc. IEEE Int. Symp. Biomed. Imag. (ISBI)*, Apr./May 2014, pp. 580–583.

[39] V. Vishnevskiy, T. Gass, G. Székely, and O. Goksel, "Total variation regularization of displacements in parametric image registration," in *Proc. Int. MICCAI Workshop Comput. Clin. Challenges Abdominal Imag.* Cham, Switzerland: Springer, 2014.

[40] E. Castillo, R. Castillo, D. Fuentes, and T. Guerrero, "Computing global minimizers to a constrained B-spline image registration problem from optimal l_1 perturbations to block match data," *Med. Phys.*, vol. 41, no. 4, 2014, Art. no. 041904.

[41] M. P. Heinrich, H. Handels, and I. J. A. Simpson, "Estimating large lung motion in COPD patients by symmetric regularised correspondence fields," in *Proc. Int. Conf. Med. Image Comput. Comput.-Assist. Intervent.* Cham, Switzerland:, Springer, 2015.

[42] T. Polzin, M. Niethammer, M. P. Heinrich, H. Handels, and J. Modersitzki, "Memory efficient LDDMM for lung CT," in *Proc. Med. Image Comput. Comput. Assist. Intervent. (MICCAI)*, in Lecture Notes in Computer Science. Cham, Switzerland: Springer, 2016.

[43] J. Rühaak *et al.*, "Estimation of large motion in lung CT by integrating regularized keypoint correspondences into dense deformable registration," *IEEE Trans. Med. Imag.*, vol. 36, no. 8, pp. 1746–1757, Aug. 2017.

[44] T. Rohlfing, "Image similarity and tissue overlaps as surrogates for image registration accuracy: Widely used but unreliable," *IEEE Trans. Med. Imag.*, vol. 31, no. 2, pp. 153–163, Feb. 2012.

[45] N. J. Tustison, B. B. Avants, and J. C. Gee, "Directly Manipulated Free-Form Deformation Image Registration," *IEEE Trans. Image Process.*, vol. 18, no. 3, pp. 624–635, Mar. 2009.

[46] A. Pai, S. Sommer, L. Sorensen, S. Darkner, J. Sporring, and M. Nielsen, "Kernel bundle diffeomorphic image registration using stationary velocity fields and Wendland basis functions," *IEEE Trans. Med. Imag.*, vol. 35, no. 6, pp. 1369–1380, Jun. 2016.

[47] Y. LeCun, Y. Bengio, and G. Hinton, "Deep learning," *Nature*, vol. 521, pp. 436–444, May 2015.

[48] I. I. Goodfellow, *Deep Learning*. Cambridge, MA, USA: MIT Press, 2016.

[49] X. Cao, J. Yang, J. Zhang, Q. Wang, P.-T. Yap, and D. Shen, "Deformable image registration using a cue-aware deep regression network," *IEEE Trans. Biomed. Eng.*, vol. 65, no. 9, pp. 1900–1911, Sep. 2018.

[50] M.-M. Rohé, M. Datar, T. Heimann, M. Sermesant, and X. Pennec, "SVF-Net: Learning deformable image registration using shape matching," in *Proc. Int. Conf. Med. Image Comput. Comput.-Assist. Intervent.* Cham, Switzerland: Springer, 2017, pp. 266–274.

[51] H. Sokooti, B. de Vos, F. Berendsen, B. P. F. Lelieveldt, I. Išgum, and M. Staring, "Nonrigid image registration using multi-scale 3D convolutional neural networks," in *Proc. Int. Conf. Med. Image Comput. Comput.-Assisted Intervent.* Cham, Switzerland: Springer, 2017, pp. 232–239.

[52] K. Ma, "Multimodal image registration with deep context reinforcement learning," in *Proc. Int. Conf. Med. Image Comput. Comput.-Assist. Intervent.* Cham, Switzerland: Springer, 2017, pp. 240–248.